ANATOMICALLY CORRECT ADAPTION OF KINEMATIC SKELETONS TO VIRTUAL HUMANS

Christian Rau and Guido Brunnett
Computer Graphics Group, Chemnitz University of Technology, Strasse der Nationen 62, Chemnitz, Germany

Keywords: Virtual Humans, Skeleton Extraction, Motion Retargeting, Character Animation.

Abstract: The adaption of a given kinematic skeleton to a triangular mesh representing the shape of a human is a task still done manually in most animation pipelines. In this work we propose methods for automating this process. By thoroughly analyzing the mesh and utilizing anatomical knowledge, we are able to provide an accurate skeleton alignment, suited for animating the surface of a virtual human based on motion capture data. In contrast to existing work, our methods on the one hand support the anatomically correct adaption of detailed skeletal structures, but on the other hand are robust against the reduction of the mesh's tessellation complexity.

1 INTRODUCTION

In order to animate a given body mesh it is necessary to fit a kinematic skeleton to the mesh. This step is crucial because flaws in the alignment will result in rather unnaturally looking movements, even if captured data is used to describe the motion. The adaption of the kinematic skeleton to the mesh is difficult for two reasons:

1. The mesh only describes the outer surface of the body. The anthropometric measures of an inscribed human skeleton are unknown.
2. The kinematic skeleton only represents an abstraction of the human skeleton, i.e. it consists only of a subset of the human joints and, furthermore, describes the flexibility of the joints, and especially the interrelations of their movements, only in an approximative way.

For these reasons the alignment of the kinematic skeleton to the mesh is usually done manually in most animation pipelines. Existing methods for automating this fitting problem are summarized in section 2. The method presented in this paper differs from the existing work in the following respects:

1. The proposed techniques are to a large extent independent of the actual topology of the kinematic skeleton and support a wide range of skeletal structures, from coarse spinal skeletons to a complete set of vertebral joints.
2. Our algorithms are rather independent of the model's posture and robust against the reduction of the mesh's tessellation, making them applicable on a wide range of input meshes.

The remainder of this paper is organized as follows: After summarizing the existing approaches for skeleton extraction and fitting in section 2, we present the proposed techniques for aligning a kinematic skeleton to an arbitrary skin mesh in section 3. The results and their discussion are given in section 4.

2 RELATED WORK

The extraction of skeletons, as a lower dimensional abstraction of a geometric model, has been studied extensively (Cornea et al., 2007). The fitting of a skeleton with a predefined topology to a given mesh requires completely different approaches, but the skeleton extraction can still guide the fitting process, as in (Baran and Popović, 2007) and (Poirier and Paquette, 2009). These methods fit a kinematic skeleton to a mesh by comparing it to an extracted geometric skeleton and thus reducing the dimensionality to a graph matching problem. Another approach has been taken in (Lu et al., 2009) by iteratively optimizing the skeleton segments' positions to correspond with the centroids of their surrounding geometry.

The problem of these methods is their generality. By not constraining themselves to models of humans, they may suffice for the manual creation of animations but lack the one-to-one correspondence of skeleton joints to real human joints. This has been

Rau C. and Brunnett G..
ANATOMICALLY CORRECT ADAPTION OF KINEMATIC SKELETONS TO VIRTUAL HUMANS.
DOI: 10.5220/0003822503410346
In *Proceedings of the International Conference on Computer Graphics Theory and Applications* (GRAPP-2012), pages 341-346
ISBN: 978-989-8565-02-0

addressed in (Dellas et al., 2007) which constrains the processed models to humans and can, therefore, utilize both the semantics of the individual skeleton joints and the knowledge about the human body. They first segment the mesh into semantic parts (like head, limbs, etc.) and then analyze the surface by means of a multi-scale curvature classification (Mortara et al., 2003). This, however, requires a quite highly tessellated mesh (e.g. body scans of real humans).

3 ANATOMICALLY CORRECT SKELETON ALIGNMENT

We assume an already roughly aligned skeleton to be given. This can be derived by one of the general fitting methods (Lu et al., 2009)(Poirier and Paquette, 2009). Furthermore, we work directly on the absolute joint positions. In this way the joint angles and segment lengths are adapted to the model implicitly and the methods can stay independent of the actual topological structure of the skeleton.

To stay independent of the orientation of the model in 3d space, all computations are done in the local body coordinate system, defined by the three orthogonal body planes: the frontal plane, separating the body into a front and a back part, the sagittal plane, separating the body into a left and a right part, and the transverse plane that separates the body into a lower and an upper part. In the following expressions as *upper* or *front* are to be understood with respect to the local body frame. If not specified a-priori, these planes could be extracted by a principal component analysis of the mesh, but due to possible asymmetries in the model's pose, this can result in a quite misaligned frame. We, therefore, base their computation only on particular parts of the body, namely the head and the legs, to reduce this pose dependence.

3.1 Extraction of Body Frame and Head Geometry

To compute the transverse body plane we use the roughly aligned skeleton as follows. For each leg we determine a vector pointing from the ankle to the hip. Assuming an upright standing human, the average of these vectors provides a reasonable approximation of the normal of the transverse plane. Now we can extract the head's geometry as a set of horizontal slices by intersecting the mesh with a sequence of planes parallel to the transverse plane, starting at the topmost point of the mesh (fig. 1, left). Because of the varying head sizes across all humans, the termination criterion

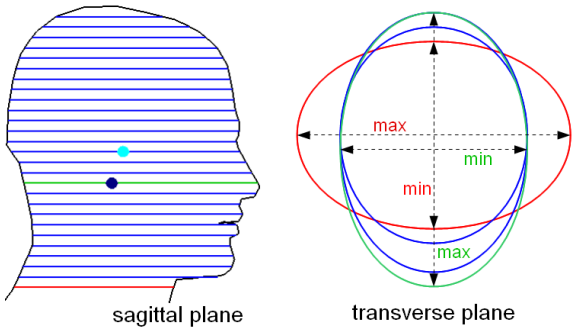

Figure 1: Termination criteria for head extraction (green: maximal slice). Chin-throat transfer marked by decrease in slice diameter (left) and head-torso transfer marked by switching principal axes (right).

for this head extraction process cannot be based e.g. on the body's height. Instead we proceed as follows. For each intersection polygon representing a slice we employ a principal component analysis to its vertices to compute the slice's diameter as the maximum expansion along its major axis. During the extraction process we keep track of the slice with the maximal diameter and check if either the diameter of the current slice has shrinked significantly compared to this maximal slice (fig. 1, left), or if it's principal axes have rotated by 90° compared to the maximal slice (fig. 1, right). The former case marks the transfer from chin to throat and the latter case marks the transfer from head to torso in general and is only needed if the former was not significant enough to be detected.

From the head geometry we can finally compute the other two body planes as follows. After projecting all the head slices' vertices into a single transverse plane, both plane normals can be computed as the principal axes of those points. Here we make use of the assumption that the human is looking straight ahead and that the head is longer in the forward direction than in the sideward direction, which is less restrictive than assuming a completely symmetrical pose of the whole body. Furthermore, the head's geometry can now be used to compute its centroid by simply taking the perimeter-weighted average of the slices' centroids.

But what we are really looking for is the position of the joint connecting the head with the spine (fig. 1, left, dark blue), which is not identical to the head's centroid (fig. 1, left, light blue). This joint is normally at the height of the nose, so we first project the centroid onto the plane corresponding to the slice with the largest forward extent (fig. 1, left, green). Now only its position inside the transverse plane needs to be adjusted slightly. By looking at a real skull cut along the transverse plane (fig. 2, right), we see that the back

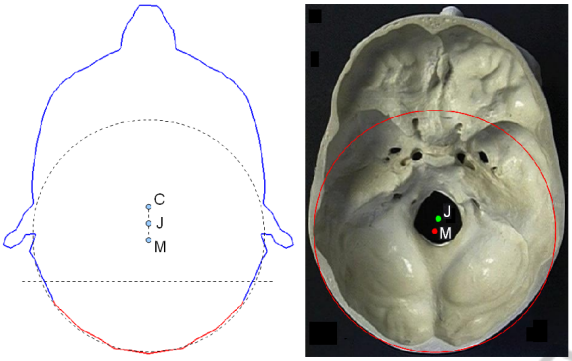

Figure 2: Joint position (J) as average of projected head centroid (C) and occipital center (M) for head slice (left) and real skull (right) (Crimando, 1998).

of the head is quite circular, with the circle's center lying near the searched joint position. Based on our observations we approximate the back of the head by a circle and compute the final joint position as the average of the projected head centroid and this circle's center point (fig. 2, left). The leaf node of the head skeleton is only used to define the skull segment and does not have an anatomical correspondence. Assuming an upright head position, it is just set to the head joint's position, translated to the cranial roof along the transverse plane's normal.

3.2 Positioning of Spinal Joints

Despite its complicated anatomical structure, the basic shape of the spine can be described by a planar curve in the median plane, the sagittal plane through the center of the torso. This curve consists of four parts with alternating signs of curvature (fig. 3a). From top to bottom these parts consist of the 7 vertebrae of the cervical spine, the 12 vertebrae of the thoracic spine, the 5 vertebrae of the lumbar spine, and the remaining 9 to 10 vertebrae that merged into sacrum and coccyx over time. In the following we will describe the steps for correctly positioning a complete set of vertebral joints, meaning the abstract joints connecting all 24 adjacent vertebrae of the upper three parts of the spine. In addition to this we also compute the center point of the sacrum as a representation of the sacroiliac part of the spine.

By observing real humans it becomes evident that the shape of the back quite closely follows the shape of the spine (fig. 3b). In conjunction with the characteristic shape of the spine curve this suggests to create the curve by deducing its points of maximal curvature from their corresponding points on the back curve and interpolating these by a simple spline curve (fig. 3c). A similar approach can be found in (Dellas et al., 2007) to extract a simple 3-segment spine, but we will take this idea further to extract the complete set of spinal joints.

First we reduce the problem domain to two dimensions by intersecting the mesh with the median plane. This results in a closed polygon which we refer to as the silhouette of the torso (fig 3c). To get a continuous representation of this silhouette and to cope with low-polygon meshes, the vertices of this piecewise linear curve are interpolated by a cubic B-spline curve, which gives a better approximation of the human shape.

Now we can extract some of the characteristic points of the torso. For this we split the silhouette at its lowest and highest points into a front and a back segment. For both segments we consider the signed distance function to the frontal plane, whose normal points forward. Now, on the back segment we define the neck point and lumbar point as local maxima of this function and the back point and sacroiliac point as local minima. For the front segment only the throat as point of minimal distance to the frontal plane and height between back and neck is of interest. The crotch is simply marked by the lowest point on the whole silhouette.

From these characteristic points, which are also shown in fig. 3c (blue), corresponding points on the spine curve (red) can be determined as follows. The joint connecting the spine with the head — computed in the previous section — represents the upper end of this curve. The center of the throat as the average of the throat and neck points is also passed by the spine and marks the beginning of the cervical spine and, therefore, the joint between *C7* and *T1*. The back and lumbar points directly correspond to specific inter-vertebral joints on the same vertical position, namely the joints connecting *T6* with *T7* and *L3* with *L4* respectively, moved from the back into the body. The amount of this movement is just a heuristical value depending on the body's overall height. The height of the sacroiliac point marks the center point of the sacrum and, together with the height of the crotch, determines the lower end of the spine curve. Once all these points have been computed, they are interpolated by a Catmull-Rom spline, to yield the final spine curve.

The remaining spinal joints' positions along the curve are determined in analogy to the size changes of the vertebrae of a real spine, by minimizing the length deviation of adjacent segments (fig. 3c). The use of a chordal parameterization for the spine curve and it's rather simple shape — that stays quite close to it's control polygon — lets us treat the parameter values as a reasonable approximation of the arc

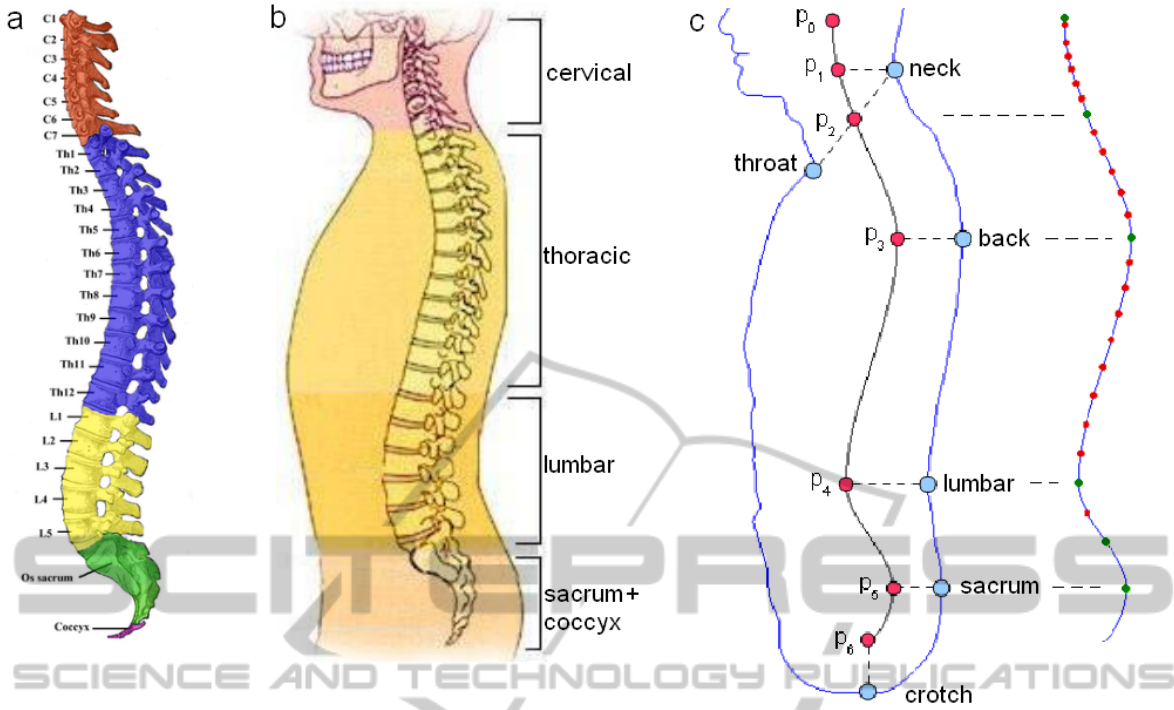

Figure 3: a) Different regions of a real spine. b) Spine with its shape closely following the back of a real human. c) Extracted spine curve for virtual human with the characteristic points guiding its construction and the final positions of the spinal joints along the curve.

length along the curve. Therefore, the positioning of the spinal joints along the curve, represented by their parameter values, can be computed by minimizing the function

$$f(\mathbf{t}) = \sum_{i=2}^{n-1} \left(t_i - \frac{t_{i-1} + t_{i+1}}{2} \right)^2 \qquad (1)$$

with t_i being the parameter of the ith inter-vertebral joint, which stays fixed for the joints corresponding to the spine curve's control points. Under the above made assumptions for the parameter values this minimization strives for a joint distribution with adjacent vertebrae having the same size.

3.3 Segmentation and Fitting of the Limbs

Although not completely anatomically correct, it is reasonable to assume the limbs' joints lying on their center lines. So the first step is to find the centroid curves for the the legs and arms, together with some more parameters describing their geometry. For this we employ the *Plumber* algorithm developed in (Mortara et al., 2004). This method extracts tubular parts — in our case the limbs — as a sequence of slices (fig. 4a), by repeatedly intersecting the geometry with spheres. In contrast to the original *Plumber* method we use the pre-aligned skeleton to define the starting point of this extraction process. For each slice the barycenter of the polygonal intersection curve, its length, and its principal diameters are computed. These barycenters are interpolated by a cubic B-spline (fig. 4a), and to gain a continuous representation of the limb's geometry the lengths and diameters are also interpolated by cubic B-splines, using the same parameterization as for the centroids.

For the positions of the hips we actually do not need this information, as they can be deduced quite easily from the previously computed characteristic points of the torso. First, their height is taken as the average of the heights of the crotch and sacroiliac points. Next, we intersect the mesh with a transverse plane at this height and use the centroids of the left and right halves of the resulting intersection curve for the hip joints' positions (fig. 4b).

Despite their similarity the shoulders have to be treated differently from the hips because of their much higher flexibility. Although their height can also be deduced from the spine, intersecting such a transverse plane with the direction of the upper arm would be very imprecise if the arms had a quite horizontal pose. Instead of this, we first search the armpit as an indicator for the shoulder position. Because it marks the connection of the arm to the torso, this is a very

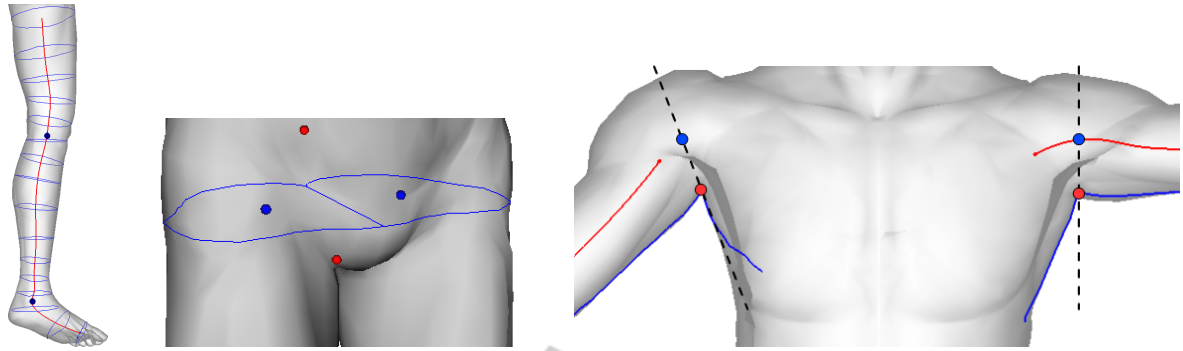

(a) (b) (c)

Figure 4: a) Computation of hip joints (blue) by intersecting the mesh with transverse plane at the height between crotch and sacroiliac points (red). b) Computation of shoulder joint (blue) by 1. determining armpit point (red) on armpit curve and 2. intersecting sagittal plane through armpit (dashed) with arm direction.

prominent geometrical feature and rather independent of the model's tessellation quality and posture. So we first find the armpit as a distinct point of high curvature (fig. 4c, red) on a surface curve running on the side of the body in the frontal plane. Now we determine the upper arm direction by approximating the upper part of the arm's centroid curve by a line and compute a sagittal plane through the armpit (fig. 4c, dashed line), half-way rotated into the arm direction. The intersection point of this plane with the approximated arm direction marks the shoulder position (fig. 4c, blue).

Because of its low flexibility, the ankle joint's position can be found by simply searching for a point of maximal curvature in the lower part of the leg's centroid curve (fig. 4a). Their arm counterparts, the wrist joints, again have to be found differently. The wrist joint marks a local minimum of the arm's thickness (measured from top to bottom) as well as a global minimum of the arm's width (measured from side to side). In the region of the wrist these values fortunately correspond to the previously computed principal diameters of the arm. So under all of the local minima of the thickness — under which could also be the palm — we use the one nearest to the global minimum of the width, or more accurately, its corresponding point on the arm's centroid curve.

The knee and elbow joint can be found in a similar way as the points on the middle parts of their respective limbs' centroid curves, that produce the smallest knee and elbow angles. If this joint position produces a very obtuse angle we instead take the point producing the optimal upper to lower limb ratio proposed in (Dellas et al., 2007) and search for a point with a slice of minimal perimeter in its vicinity (fig. 4a).

4 RESULTS

After carrying out the described joint positioning processes we have a detailed skeleton, adapted to the geometric model of a human (fig. 5). For the left model in fig. 5 we can compare the automatically computed skeleton to a reference skeleton, which was fitted manually by an expert in biomechanics. The average and maximum differences in joint position over all optimized joints, compared to this reference skeleton, are 14 mm and 29 mm respectively, which shows the accuracy of our methods.

By comparing the fitting results for differently detailed versions of the same model (from 3,000 to 81,000 triangles) to the results on the version with 11,000 triangles (tab. 1), we see that the average differences in joint position are at maximum 5 mm, which shows the algorithms' independence from the overall tessellation quality of the meshes. But it has to be noted, that the geometry analyses, especially the spine recognition, might be distorted by too loose-fitting clothes, possibly requiring manual adjustments.

In fig. 6 we can see a very roughly aligned skeleton and the final result of our adaption based on this pre-alignment. The apparent high quality of the alignment is due to the fact that the input skeleton is actually only used to guide the segmentation of the leg and arm geometries. This figure also shows the pose

Table 1: Average differences in joint position for differently tessellated versions of the same model, compared to the results obtained on a model with 11,000 triangles.

#Δ	6k	19k	32k	49k	81k
ε in mm	3.54	0.72	1.30	4.04	5.06

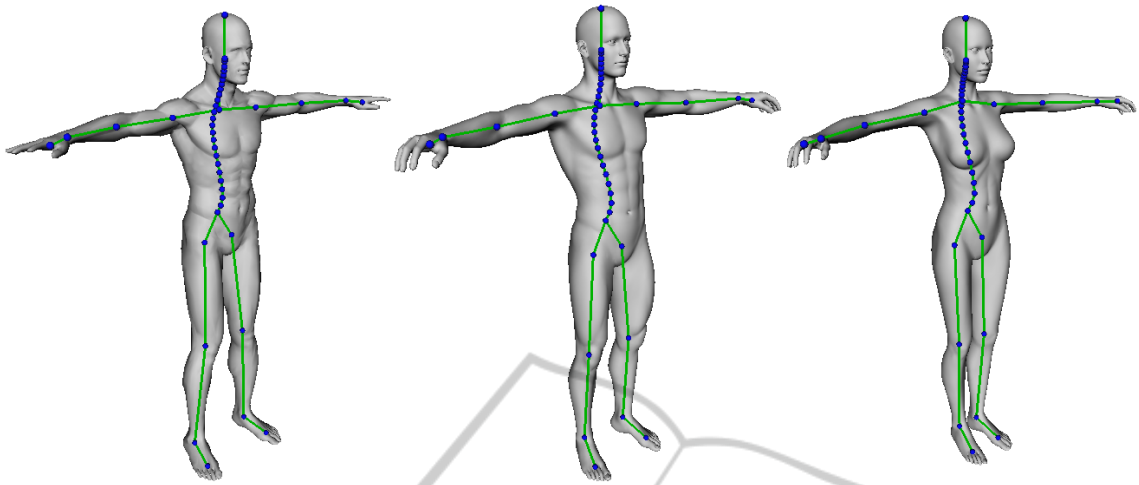

Figure 5: Skeleton fitting results for different human models.

independence of the proposed approach, as the average difference in segment length compared to the undeformed model's skeleton is only 9 mm. But this pose independence has its limits as the torso has to be upright, for the spine recognition not to fail. And in this particular case the body frame had to be specified manually because the model neither stands on both legs nor looks straight forward.

The fact that the skeleton fitting did not take longer than half a second (measured on a *Pentium 4* with 3 GHz) for all tested models, which had up to 81,000 triangles, is sufficient to show its efficiency, assuming an absent real-time requirement anyway.

To finally use the skeleton for animating the mesh there still needs to be made a connection between both by computing the segments' influences on the vertices. This can be achieved by the method presented in (Baran and Popović, 2007). Together with the pre-alignment of (Lu et al., 2009) or (Poirier and Paquette, 2009) and the proposed joint optimization we get a nearly automatic pipeline for making an arbitrary human model animation-ready.

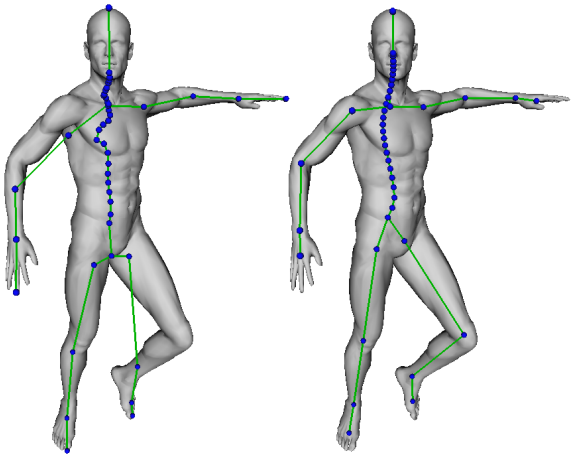

Figure 6: Left: very rough skeleton alignment (based on (Poirier and Paquette, 2009)). Right: optimized skeleton based on this pre-alignment.

REFERENCES

Baran, I. and Popović, J. (2007). Automatic rigging and animation of 3d characters. *ACM Transactions on Graphics*, 26(3):72.

Cornea, N. D., Silver, D., and Min, P. (2007). Curve-skeleton properties, applications, and algorithms. *IEEE Transactions on Visualization and Computer Graphics*, 13(3):530–548.

Crimando, J. (1998). Skull anatomy tutorial.

Dellas, F., Moccozet., L., Magnenat-Thalmann, N., Mortara, M., Patané, G., Spanguolo, M., and Falcidieno, B. (2007). Knowledge-based extraction of control skeletons for animation. In *SMI '07: Proceedings of the IEEE International Conference on Shape Modeling and Applications 2007*, pages 51–60.

Lu, L., Lévy, B., and Wang, W. (2009). Centroidal voronoi tessellations for line segments and graphs. Technical report, INRIA - ALICE Project Team.

Mortara, M., Patanè, G., Spagnuolo, M., Falcidieno, B., and Rossignac, J. (2003). Blowing bubbles for multi-scale analysis and decomposition of triangle meshes. *Algorithmica*, 38(1):227–248.

Mortara, M., Patanè, G., Spagnuolo, M., Falcidieno, B., and Rossignac, J. (2004). Plumber: a method for a multi-scale decomposition of 3d shapes into tubular primitives and bodies. In *SM '04: Proceedings of the ninth ACM symposium on Solid modeling and applications*, pages 339–344, Aire-la-Ville, Switzerland.

Poirier, M. and Paquette, E. (2009). Rig retargeting for 3d animation. In *GI '09: Proceedings of Graphics Interface 2009*, pages 103–110, Toronto, Ont., Canada.